Environmental Science Processes & Impacts

ROYAL SOCIETY OF CHEMISTRY

PAPER

Cite this: *Environ. Sci.: Processes Impacts*, 2024, **26**, 323

Isolation of aqueous pesticides on surface-functionalized SBA-15: glyphosate kinetics and detailed empirical insights for atrazine†

Paul N. Diagboya, *[a] Johannes Junck,[a] Samson O. Akpotu[b] and Rolf-Alexander Düring[a]

Atrazine and glyphosate are two of the most used pesticides around the world causing serious water contamination. In this study, amine-functionalized Santa Barbara Amorphous-15 silica (SBA-15-NH_2) was synthesized and employed for the aqueous adsorption of atrazine and glyphosate. The adsorbent was mesoporous post-functionalization with lower surface area, pore volume, size, and stability when compared to the SBA-15. The pesticides adsorption rates were high with over 85% of potential adsorption having occurred within the initial 180 min. The equilibria for atrazine and glyphosate adsorption were 60 and 360 min, respectively, and the rate data fit the fractal pseudo-second-order and pseudo-second-order models, respectively. Atrazine adsorption was higher at lower solution pH with reduced adsorption as the pH value increased. There was enhanced atrazine adsorption as temperature increased from 22 to 32 °C, but further temperature rise resulted in lower adsorption compared to that recorded at 22 °C. The processes comprise electrostatic interaction, trapping of atrazine within mesopores, and multi-layer adsorption of atrazine on surface-adsorbed atrazine. The equilibrium data fitted the Langmuir adsorption isotherm model better than the Freundlich. The SBA-15-NH_2 adsorption capacity for atrazine and glyphosate was better than many adsorbents reported in literature, the adsorbent is reusable, and exhibited sustained efficiencies for atrazine that was ≥82% even after 3-cycles, an indication of chemical stability and renewability.

Received 28th September 2023
Accepted 18th December 2023

DOI: 10.1039/d3em00425b

rsc.li/espi

Environmental significance

The need for higher agricultural yields has led to the continuous contamination of freshwater sources by pesticides. This is of particular interest due to the unintended consequences (on human and ecosystem health) of the ever-increasing environmental pesticide input. Though at trace levels, an estimated 90% of global source waters are contaminated and the elimination of contaminants from potable water is seemingly intractable. Atrazine and glyphosate are among the most prevalent water contaminants, causing serious concerns due to their effects on the ecosystem and humans. In fact, the International Agency for Research on Cancer (IARC) has re-classified glyphosate as a Category 2A carcinogen. In order to reduce their associated disease burden in contaminated water, especially at environmentally relevant concentrations, the removals of both contaminants were studied.

Introduction

The need for higher agricultural yields has led to the continuous contamination of freshwater sources by pesticides. This is of particular interest due to the unintended consequences (on human and ecosystem health) of the ever-increasing environmental pesticide input.[1–3] An estimated 90% of global source waters are contaminated and the elimination of contaminants from potable water is seemingly intractable.[4] To reduce the disease burden associated with contaminated water, it is vital to address this global challenge.[4,5]

Atrazine and glyphosate are two of the most used pesticides around the world causing serious water contamination.[5,6] Atrazine (2-chloro-4-ethylamino-6-isopropyl amino-1,3,5-triazine) is a pre-emergent herbicide with low water solubility at 26 °C and far lower potable water permissible limit (US EPA) of ≈34 mg L^{-1} and ≈3 μg L^{-1}, respectively. However, several toxic effects on females have been observed even at exposures far lower than this permissible limit (0.7 μg L^{-1}); these include irregular menstrual cycles, significantly low estrogen levels which may lead to infertility, delayed puberty, pregnancy loss, and low birth weight.[6] On the other hand, glyphosate is a systemic and non-selective post-emergent herbicide that blocks the plant's shikimate pathway necessary for the synthesis of tryptophan, phenylalanine, and

[a]*Institute of Soil Science and Soil Conservation, Justus Liebig University, Giessen, Germany. E-mail: pauldn2@yahoo.com*

[b]*Department of Chemistry, Vaal University of Technology, Vanderbijlpark, South Africa*

† Electronic supplementary information (ESI) available. See DOI: https://doi.org/10.1039/d3em00425b

tyrosine (aromatic amino acids). These amino acids are precursors for the synthesis of vital biomolecules such as benzoic acids, lignin, alkaloids, flavonoids, and vitamin K.[5,7] Glyphosate and its metabolite (amino-methyl-phosphonic acid – AMPA) are continuously detected in environmental media,[5,8,9] and there are currently serious concerns about their effects on the ecosystem and humans. In fact, the International Agency for Research on Cancer (IARC) has re-classified glyphosate as a Category 2A (probable human) carcinogen.[10,11] The aforementioned have resulted in serious concerns for the continued use of these pesticides and have led to the need to eliminate both contaminants from water, especially potable water.

Globally, there is a rise in the usage and release of both contaminants into environmental waters, and conventional water purification methods are not effective for the decontamination of source waters due to the occurrence of contaminants at very low concentrations.[12] Adsorption is a suitable alternative for contaminants' removal from water due to its many techno-economic and environmental advantages such as low cost and varieties of adsorbents, easy preparation of adsorbents, less generation of toxic sludge, easy operation, reusability, minimal energy use, environmentally friendliness, and adsorption sites can be easily tailored towards specific contaminants.[13–16] The latter is very interesting for porous silica materials because specific tailoring yields superior adsorbents making them specifically useful in water treatment.[4,17–19] Mesoporous silica materials with high surface areas are well suited for such specific efficiency tailoring because they meet several criteria for adsorbent selection including cost efficiency, large surface area, good thermal stability, and reusability.[18] Thus, SBA-15 silica was employed for this study. It possesses surface hydroxyl groups that are not very reactive or useful for adsorption but can be easily functionalized with a more reactive amine functional group to yield amine-SBA-15 (SBA-15-NH_2). Such silica based materials and similar functionalization technologies have been reported for the adsorption of different contaminants including metals, dyes, and pharmaceuticals.[20] Though similar adsorbent has been studied for the adsorption of various aqueous contaminants,[14] to the best of our knowledge, these important pesticides have been seldom studied.[21] Recently, SBA-15-NH_2 was reported to effectively adsorb the anti-parasitic agent ivermectin especially at low aqueous concentrations and with good stability upon reuse.[17] Following the success of that study and since ivermectin is not as prevalent in water as these contaminants, the objective of this study was to use SBA-15-NH_2 for the adsorption of low and environmentally feasible concentrations of atrazine and glyphosate from aqueous solutions, test the adsorbent reusability, and explain the experimental data using various adsorption models. Testing of adsorbents for adsorption at low concentrations is vital because these contaminants are found in water at quite low concentrations.

Experimental

Synthesis and amine functionalization of SBA-15, and characterization

Milli-Q system purified water (pH 7 ± 0.2) and analytical grade chemicals were used throughout this study. The chemicals employed for the study include Pluronic P123 ($EO_{20}PO_{70}EO_{20}$) (Aldrich), tetraethyl orthosilicate (TEOS) (Acros Organics), (3-aminopropyl)-triethoxysilane (APTES) (Acros Organics), atrazine (Sigma-Aldrich) and glyphosate (Sigma-Aldrich). HPLC-grade acetonitrile (ACN) (from BDH) was used throughout the study.

The SBA-15 was synthesized[18] by hydrolyzing 2.1 g of TEOS for 1 h at 40 °C under stirring in 1.0 g Pluronic P123 dissolved in 30 mL 2 M HCl. Millipore Milli-Q H_2O (30 mL) was added followed by stirring for 20 h at 40 °C, then aging under static conditions (24 h at 87 ± 1 °C). The product was washed with Milli-Q H_2O over filter paper, air dried, and the Pluronic P123 template was removed by calcination (550 °C and 4.5 h). Functionalization to add the amine group from the APTES was carried out *via* post-synthetic modification of the calcined SBA-15. The SBA-15 was initially dispersed in toluene (80 mL) before adding APTES (4 mL) under reflux (5 h at 110 °C). The product (SBA-15-NH_2) was washed with ethanol three times and dried at 35 °C for 3 h.

The SBA-15 adsorbents were characterized using Fourier transform infrared spectrometer (FTIR) (Nicolet iS50 FT-IR Thermo Scientific) (scanning from 4500 to 450/cm), X-ray powder diffraction (XRD) spectrometer (D8 Advance Bruker AXS, Germany) (Cu Kα radiation; 2 theta range of 0.5–2.5° and 10–80°), Quantachrome Quadrasorb (Florida) for the Brunauer–Emmett–Teller (BET) surface area from the N_2 adsorption–desorption isotherm (degassed at 80 °C before nitrogen adsorption–desorption), Thermo-gravimetric analyzer (TGA) (Perkin-Elmer TGA 4000, USA) (heating at 5 °C min^{-1} up to 900 °C in nitrogen), Scanning Electron Microscope (SEM) (Zeiss Auriga Field Emission), and high resolution transmission electron microscopy (HRTEM, JEOL 2100, Japan). The adsorbent pH in water and 1.0 M KCl as well as the pH at point zero charge (pHpzc) were determined.[22]

Atrazine adsorption studies and experimental data treatment

Atrazine and glyphosate stock solutions (1000 mg L^{-1} each) were prepared in 20/80% ACN/water and Milli-Q water, respectively, stored at 4 °C and used throughout this study. Serial dilutions for atrazine (in 0.01 M $CaCl_2$) and glyphosate (in 0.1 M KCl) for each working solution were made from these stocks. Sodium azide (100 mg L^{-1}) was used as a biocide throughout the study to inhibit microbial growth and degradation of the contaminants.

It has been reported[23] and also observed in the preliminary experiment that atrazine and glyphosate adsorption on pristine SBA-15 were not significant, thus the study focused on SBA-15-NH_2. Replicate batch adsorption studies for both contaminants were carried out by employing 20 mg mass of SBA-15-NH_2 in a specific volume of contaminant solution (atrazine 20 mL and glyphosate 10 mL) and incubating for 1440 min in an orbital shaker (200 rpm) until withdrawal at equilibrium, then centrifugation at 870 RCF (2000 rpm)/10 min and filtration using 0.45 μm syringe PES filters. The rates of adsorption at varying times (1–1440 min) were determined for atrazine (≈3500 μg L^{-1}) and glyphosate (≈20 000 μg L^{-1}), while the effects of atrazine solution pH (3–11), atrazine concentration (200–4000 μg L^{-1})

and ambient temperature (22–42 °C), as well as reusability of SBA-15-NH_2 for atrazine re-adsorption, were studied. The pH of contaminants solutions was adjusted using 0.1 M NaOH or HCl where needed. A reuse test on SBA-15-NH_2 was conducted by decanting the contaminant solution and the residue adsorbent washed twice using 100% ACN in an electronic shaker for 2 h at 200 rpm, centrifuged, carefully decanted, dried for 5 h at 50 °C and reapplied for adsorption using 20 mg and 20 mL atrazine solution of ≈220 μg L^{-1}. This reuse cycle was repeated twice.

The concentrations of atrazine and glyphosate remaining in the solution were determined by HPLC-DAD (1200 Series, Agilent Technologies Inc., USA) and HPLC-MS (Thermo Scientific), respectively. The HPLC-DAD was fitted with a G1316A column oven, G1329A autosampler, G1311A quaternary pump, and G1315B diode array detector (DAD). The mobile phase was 57 : 43 ACN (0.5% water) : water (water contains 10% ACN), the column temperature was 35 °C, flow rate of 0.3 mL min^{-1} at an injection volume of 40.0 μL, a wavelength of 223 nm and run time was 6 min with a retention time of 2.8 min, while after every 20 samples, the column was cleaned by flushing starting from 53% ACN up to 90% ACN.

Glyphosate quantification followed a reported protocol[24] using HPLC (Thermo Scientific) coupled to MS (Thermo Scientific Exactive Orbitrap) detector (HPLC-MS). Chromatographic separation was done on Thermo Scientific 600 Pump with Waters *X*-Bridge C18 3.5 μm column, 150 mm × 2.1 mm inner diameter kept at 27 °C. Ammonium acetate (5 mM) and methanol were used as mobile phases A and B, respectively, while separation (in 5 min) followed the gradient program: 0–30 s, 90 : 10 (A : B); 30–90 s from 90 : 10 to 5 : 95 (A : B); 90–100 s from 5 : 95 to 0 : 100 (A : B); 100–200 s 0 : 100 (A : B); 200–300 s 90 : 10 (A : B). A flow rate of 300 μL min^{-1} was used with an injection volume of 10.0 μL, while the equipment was on the negative ion mode at a scan mass range of 50–450 *m*/*z*.[24] The quantitation was done by monitoring the primary transitions at *m*/*z* 168 (glyphosate) and *m*/*z* 110 (AMPA), while the data were acquired and processed using Thermo Xcalibur Roadmap™ software.

The quantities (q_e) of atrazine and glyphosate adsorbed (μg g^{-1}) were determined by using eqn (1)

$$q_e = (C_O - C_e) \times v/m \quad (1)$$

The variables C_o, C_e, m, and v are the contaminant concentrations (mg L^{-1}) at start and equilibrium, SBA-15-NH_2 mass (μg), and volume (mL) of solution used, respectively.

The rates of adsorption data and the predicted process mechanism were described using OriginPro 2015 (OriginLab Corporation, Northampton, MA, USA) calculated parameters from three nonlinear adsorption kinetics models: Pseudo-First Order (PFO), Pseudo-Second Order (PSO), and the homogeneous Fractal Pseudo-Second Order (FPSO)[25] (ESI 1†). Still using OriginPro 2015, the atrazine equilibrium adsorption data of the various temperatures were fitted and described using 2 simplistic adsorption isotherm models (Langmuir[26] and Freundlich[27]) (ESI 1†).

To determine the thermodynamics, atrazine equilibrium adsorption data obtained between 22 and 42 °C were evaluated using the equilibrium constants (K_c) at varying temperatures and energy parameters (Gibbs free energy $\Delta G°$, entropy change $\Delta S°$ and enthalpy change $\Delta H°$) following the equations in eqn (2)–(5). Dimensionless K_c was computed from eqn (2) (ref. 28 and 29) where M_A is the molar weight of the atrazine (215.68 g mol^{-1}) (this holds true when the experimental concentrations are expressed in mg L^{-1}), b is the Langmuir constant (best fitting adsorption isotherm as observed below), and γ_e is activity coefficient. For non-ionic or ionic but dilute solutions, the activity coefficient (γ_e) is taken as unity, and eqn (2) can be approximated to eqn (3).

$$K_C = \frac{bM_A}{\gamma_e} \quad (2)$$

$$K_C = bM_A \quad (3)$$

$$\ln K_C = \ln(bM_A) = \frac{\Delta S°}{R} - \frac{\Delta H°}{RT} \quad (4)$$

$$\Delta G° = -RT \ln K_C \quad (5)$$

Results and discussion

SBA-15-NH_2 physicochemical characteristics

The SBA-15-NH_2 employed for this study has been previously characterized and described.[17] Briefly, after the functionalization, the SBA-15-NH_2 remained mesoporous and retained the type IV adsorption–desorption isotherm of the SBA-15 but the aminopropyl silane moiety blocked some of the pores within the SBA-15-NH_2 hence there was a reduction in the pore size, volume, and surface area. The BET surface area of the SBA-15-NH_2 (Table 1; Fig. 1a) is ≈2.8 fold smaller than that of the pristine SBA-15 (539 m^2 g^{-1}), while the pore volume and size were ≈2.3 and 23 times smaller, respectively. This is an indication that the coupled amine moieties were present on the mesopores of the pristine SBA-15 and blocked some of the pores, thus reducing the surface area and consequently the nitrogen adsorption. The distinctive hydroxyl group broad band

Table 1 Selected physicochemical properties of the adsorbents

Adsorbent	Surface area (m^2 g^{-1})	Pore volume (cm^3 g^{-1})	Pore size (nm)	pH in H_2O	pH in 1 M KCl	pHpzc
SBA-15	539	0.848	6.010	6.1 ± 0.2	5.0 ± 1.1	2.1
SBA-15-NH_2	192	0.376	0.260	8.9 ± 0.1	9.2 ± 0.4	4.9

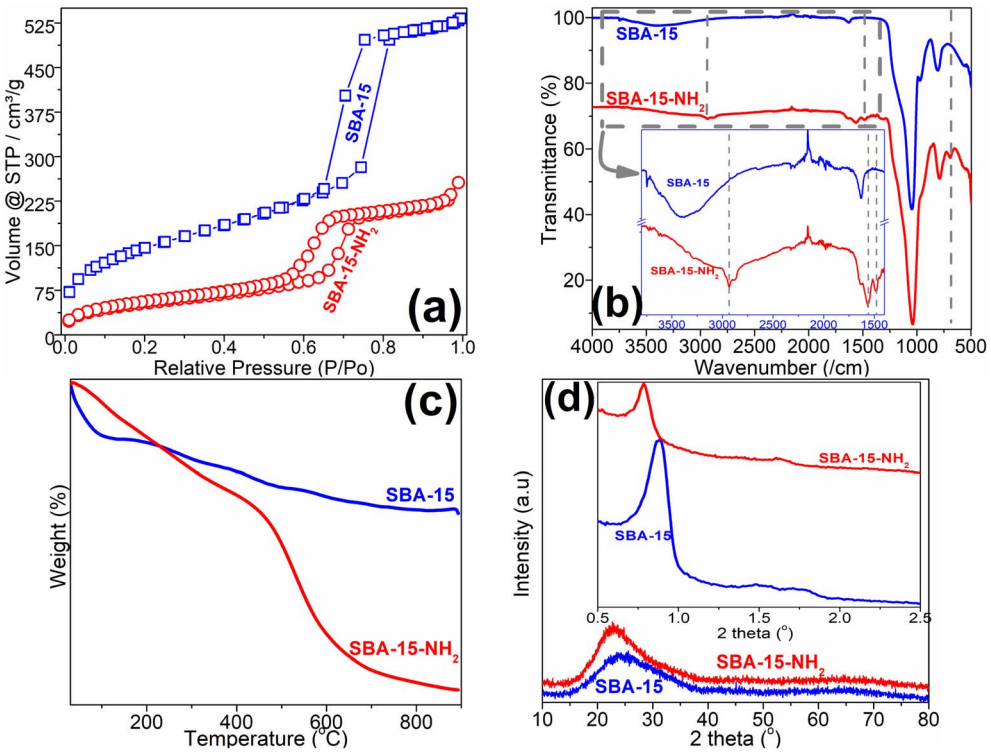

Fig. 1 (a) N_2 adsorption and desorption isotherms at 77 K; (b) SBA-15 and SBA-15-NH_2 FTIR spectra peaks of [inset: enlarged spectra section from 3000 to 1400 cm^{-1}]; (c) TGA spectra for SBA-15 and SBA-15-NH_2; (d) high-angle XRD diffractograms [inset: low-angle XRD diffractograms].

of silanol on the SBA-15 at 3460 cm^{-1} (Fig. 1b) disappeared post-functionalization, marking the point of attachment of the aminopropyl silane moiety onto the SBA-15.[17] The functionalization introduced stronger amide–I vibrations at 1560 cm^{-1} (Fig. 1b inset),[30,31] while the APTES stretching vibrations of $-CH_3$ and $-CH_2$ groups were observed at 2940 cm^{-1}.[30] The SBA-15-NH_2 exhibited lower stability ($\approx$22%) than the pristine SBA-15 ($\approx$12%) at $\geq$600 °C (Fig. 1c), a situation attributed mainly to the decomposition of the attached APTES organic moiety. The introduction of this moiety did not affect the basic lattice configuration or the usual high-angle XRD 2θ reflection at 22° for amorphous SiO_2 (Fig. 1d). Similarly, low-angle XRD reflections (100, 110, and 200 diffraction planes) below 2° typical of well-organized pore structures of SBA-15 were unaffected. The pH of the SBA-15 in water or KCl was slightly acidic ($\approx$6), while post-functionalization it became alkaline ($\approx$9) (Table 1), suggestive of the adsorbent's electron donation potential. The pH at point of zero charge (pHpzc) increased in the SBA-15 from $\approx$2.1 to 4.9 in the SBA-15-NH_2.[30,31] The SBA-15 and SBA-15-NH_2 SEM and TEM images are presented in Fig. 2a–d, respectively. Smoother surfaces were observed for the SBA-15 than the SBA-15-NH_2 which was rougher due to the surface coupling of the APTES moieties. The morphological image of the SBA-15 obtained with the HRTEM was typically unchanged post-modification with the APTES, and it showed that the SBA-15 exhibited a 2-D (p6mm) ordered hexagonal symmetry with uniform and identical mesopores similar to a honeycomb.

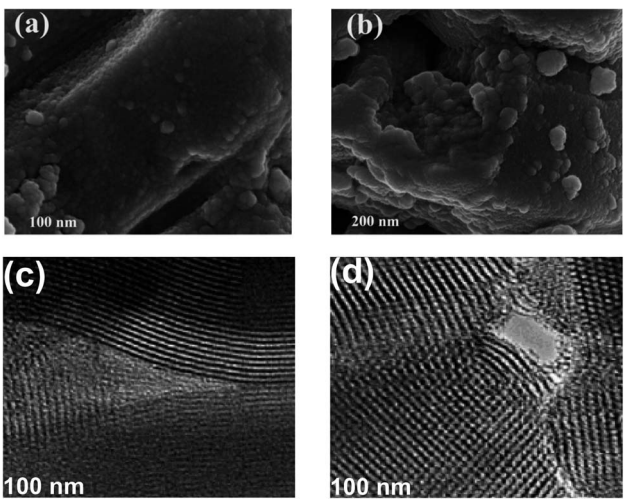

Fig. 2 SEM images of (a) SBA-15, (b) SBA-15-NH_2; HRTEM images of (c) SBA-15, and (d) SBA-15-NH_2.

Atrazine and glyphosate kinetics study

A preliminary adsorption experiment to ascertain and compare the adsorption potentials of SBA-15 and SBA-15-NH_2 (results not presented) showed that, unlike SBA-15-NH_2, pristine SBA-15 expressed no significant adsorption for both atrazine and glyphosate. Hence, only SBA-15-NH_2 was employed for further adsorption studies. Initially, the rates of atrazine (Fig. 3a) and glyphosate (Fig. 3b) adsorption by SBA-15-NH_2 were investigated over a 24 h period, and insights into the mechanism(s) of

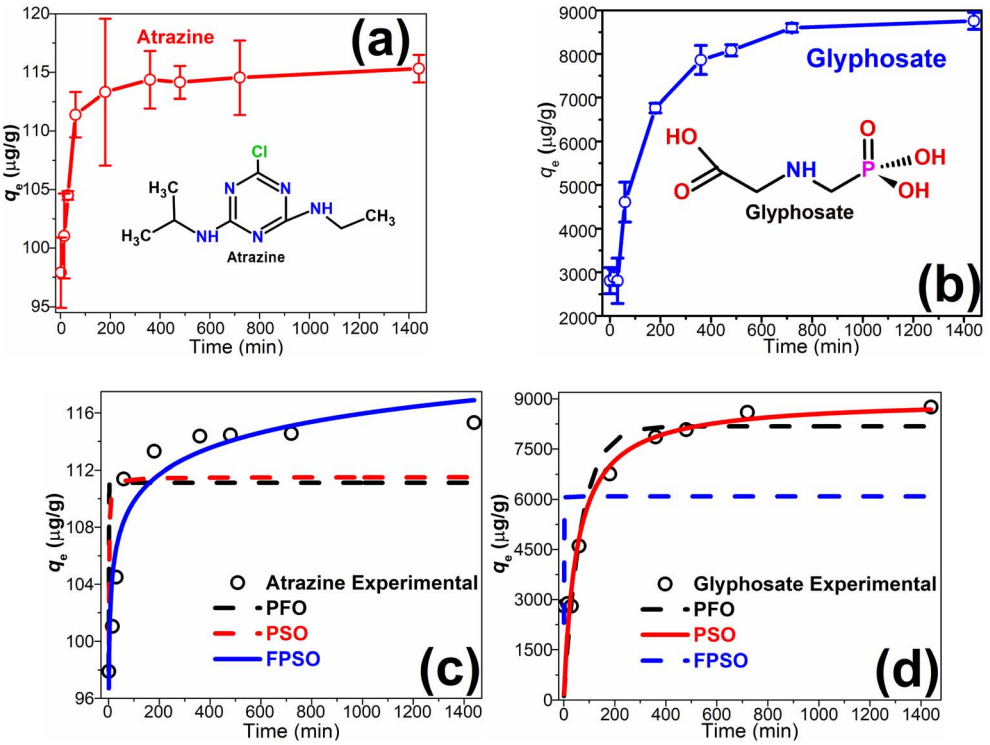

Fig. 3 (a) Atrazine adsorption rate trends (inset: atrazine structure); (b) glyphosate adsorption rate trends (inset: glyphosate structure); kinetics models' fittings for the experimental data of (c) atrazine; (d) glyphosate (experimental conditions: 20 mg SBA-15-NH_2, ≈22 °C, ≈3500 μg L^{-1} of atrazine (or ≈20 000 μg L^{-1} of glyphosate), and pH ≈6.5).

Table 2 Atrazine and glyphosate adsorption kinetics models parameters

Model of kinetics	Parameter	Atrazine	Glyphosate
PFO	q_e [μg g^{-1}]	111.1	8179.2
	k_1 [/min]	2.129	0.015
	r^2	0.355	0.788
	χ^2	28.76	1.45×10^{-6}
PSO	q_e [μg g^{-1}]	111.5	8990.9
	k_2 [g μg^{-1} min^{-1}]	0.059	2.15×10^{-6}
	r^2	0.439	0.831
	χ^2	25.02	1.15×10^{-6}
FPSO	q_e [μg g^{-1}]	170.1	6089.9
	k_f	0.008	1.00×10^{-4}
	α	0.070	3.037
	r^2	0.872	0.0837
	χ^2	5.70	7.42×10^{-6}

both atrazine and glyphosate adsorption were obtained by fitting the rate data to the PFO, PSO, and FPSO kinetics models (Fig. 3c and d; Table 2).

The proximity of the correlation coefficient (r^2) values to unity and the low chi-square (χ^2) values showed that the FPSO model ($r^2 \geq 0.87$ and $\chi^2 = 5.7$) fits the atrazine data, while the PSO model ($r^2 \geq 0.83$ and $\chi^2 = 1.15 \times 10^{-6}$) fitted the glyphosate data better than other models. This suggests the appropriateness of these models to describe the process. For the atrazine adsorption, the FPSO implies that the adsorption process was of a complex type,[32] and considering the porous nature of the SBA-15-NH_2 adsorbent, the charged amine group, and possibly ionized atrazine (Fig. 3a inset), the process is likely to comprise electrostatic interaction, trapping of atrazine within mesopores, and multi-layer adsorption of atrazine on surface adsorbed atrazine. The glyphosate adsorption data which fits better the PSO suggested a process that was mainly controlled by electrostatic interaction.[4,33] This is reasonable considering the positively charged amine group of the porous SBA-15-NH_2 and the negatively charged carboxyl and phosphate groups of the glyphosate molecule (Fig. 3b inset).

The experimental data trends depicted in Fig. 3a and b showed fast adsorption for both pesticides within the initial 180 min with over 85% of potential adsorption having occurred. The times needed to attain equilibrium for atrazine and glyphosate adsorption were 60 and 360 min, respectively. These fast adsorption rates as the process commenced were attributed to the high percentage of vacant adsorption sites on the SBA-15-NH_2 compared to the contaminant molecules in solution leading to the steepness of the curves. As the vacant adsorption sites reduced over time, the rates of adsorption slowed considerably until it equaled desorption, and hence the plateaus appeared.

Further adsorption studies on atrazine

Ambient solution pH is a vital parameter that can affect the surface charge density of the SBA-15-NH_2 adsorbent, as well as the ionization of the atrazine molecules in solution, and ultimately the adsorption;[34–37] thus the effect of solution pH on the

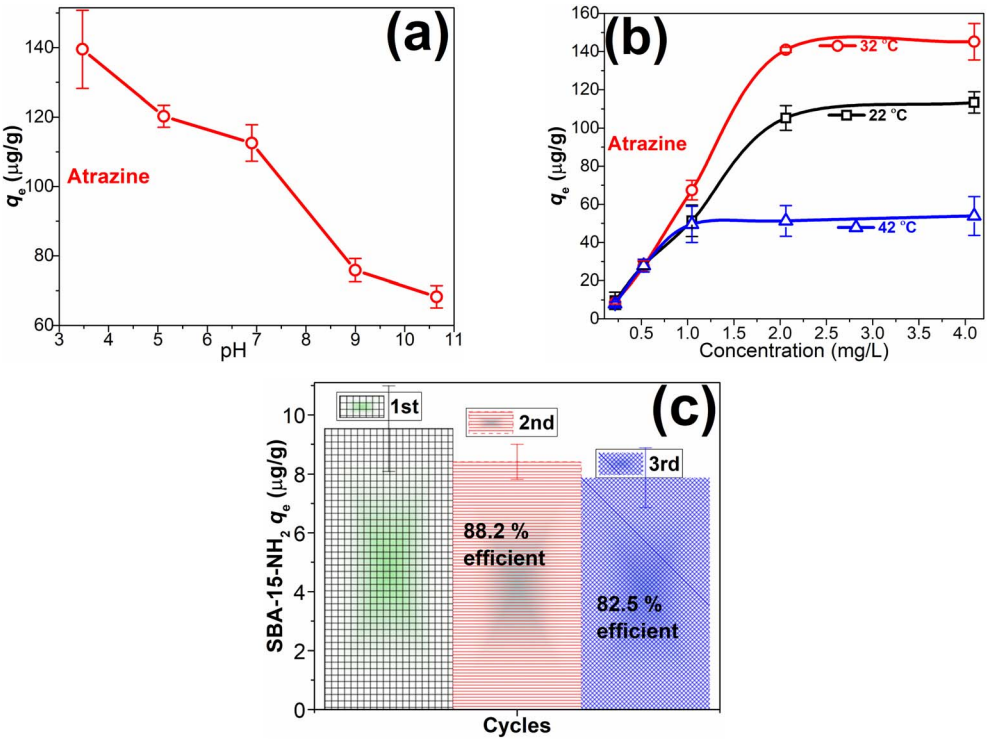

Fig. 4 (a) Atrazine adsorption trend with variation in solution pH (experimental conditions: 20 mg SBA-15-NH_2, ≈22 °C, ≈3500 μg L^{-1} of atrazine, and 1440 min); (b) equilibrium adsorption trends of atrazine at different temperatures (22, 32, and 42 °C) (experimental conditions: 20 mg SBA-15-NH_2, 1440 min, and pH ≈6.5); (c) SBA-15-NH_2 reusability for atrazine adsorption (experimental conditions: 20 mg SBA-15-NH_2, ≈3000 μg L^{-1} of atrazine, 1440 min, and pH ≈6.5).

adsorption process was investigated within the pH range of 3–11. The atrazine adsorption trend (Fig. 4a) on the SBA-15-NH_2 adsorbent expressed strong pH dependence and showed higher adsorption at lower solution pH with reduced adsorption as solution pH values were raised. Similar trends have been reported for silica gel[38] and vermiculite.[39] This trend supports the hypothesis that electrostatic attraction involving ionized atrazine species was involved in the atrazine sequestration process.

The major reason for this trend may be ascribed to the effect of varying solution pH on the SBA-15-NH_2 adsorbent and the atrazine molecules. It has been reported that at lower solution pH (below 5), approximately 50% of the ethylamino side chain of the atrazine acts as a hydrogen-bond donor while the amine of the SBA-15-NH_2 (below its pHpzc) acts as a hydrogen-bond acceptor; these conditions facilitate electrostatic interaction between both groups in the form of hydrogen bonding, and leads to the high adsorption.[34] This is in addition to the trapping of atrazine within the SBA-15-NH_2 mesopores and the possible multi-layer adsorption of atrazine on surface adsorbed atrazine facilitated by π–π interactions between aromatic atrazine rings.[37,40] However, upon raising the solution pH between 5 and 9, atrazine loses its proton and the molecules are uncharged. Hence, the initial contribution of electrostatic attraction (and the resulting π–π interactions) to the adsorption process is almost eliminated and this significantly reduces the recorded adsorption by more than half.[34] This trend is also enhanced by the deprotonation of the amine group of the SBA-15-NH_2 which makes the adsorbent almost neutral and unattractive to the atrazine molecules.

Atrazine equilibrium adsorption trends derived by varying concentrations between 0.2–4.0 mg L^{-1} and varying temperatures (22–42 °C) are presented in Fig. 4b. The adsorption process was concentration-dependent up until the concentration of 2 mg L^{-1} and then showed a distinct plateau at higher concentrations, and this is the same for all temperatures studied. A similar observation as concentration gradually increased has been reported earlier.[35] The observed trend below the atrazine concentration of 2 mg L^{-1} (Fig. 4b) may be ascribed to adsorption *via* electrostatic interactions and subsequently to the multi-layer formation that was facilitated by π–π interactions.[41,42] However, once the adsorption sites are saturated, no further adsorption occurs even at higher atrazine concentrations, resulting in the plateau.

Atrazine equilibrium adsorption trends at varying temperatures are also depicted in Fig. 4b and it was observed that there was enhanced adsorption as ambient temperature increased from 22 to 32 °C. However, a further increase in temperature (to 42 °C) resulted in lower adsorption compared to that recorded at 22 °C. The initial enhanced adsorption suggested that the process was endothermic, requiring external energy input to break the energy barrier required for further adsorption to occur. The reduced adsorption on further energy input may be ascribed to the low $\triangle H^{o}$ energy associated with some pesticides adsorption[17,43] (also reported here) which is easily broken at

Table 3 Isotherm modeling parameters for atrazine adsorption

Adsorption isotherm	Parameter	22 °C	32 °C	42 °C
Langmuir model	Q_o [μg g^{-1}]	189.6	253.0	67.2
	b	4.4×10^{-4}	4.15×10^{-4}	0.002
	r^2	0.925	0.884	0.859
	χ^2	159.4	462.4	55.49
Freundlich model	k_F	0.829	0.899	2.97
	N	0.604	0.627	0.363
	r^2	0.859	0.809	0.664
	χ^2	299.9	763.8	132.1

Table 4 Atrazine adsorption thermodynamics parameters

Parameter		Atrazine
$\Delta H°$	kJ mol^{-1}	57.8
$\Delta S°$	J mol^{-1} K^{-1}	174.0
$\Delta G°$ (kJ mol^{-1})	288.15 K	5.78
	298.15 K	6.12
	307.15 K	2.20

higher temperatures. Similar trends have been reported earlier.[17,44]

To garner further details on the adsorption process, the equilibrium adsorption data at various temperatures were fitted to the Langmuir and Freundlich adsorption isotherm models. The calculated adsorption isotherm parameters (Table 3), especially the r^2 and χ^2 values, suggest that the experimental data fitted the Langmuir adsorption isotherm model better than the Freundlich. This indicates adsorption on sites with similar affinity for atrazine. Though monolayer adsorption is implied by the Langmuir model, the good fit of the rate data to the FPSO model (previously discussed) which suggested multilayer adsorption as part of the adsorption process may mean that the energy of adsorption of the multilayer is similar in size to that of the main surface electrostatic adsorption. This phenomenon is similar to the distributed reactivity of the various sorption points within the adsorbent.[45] The calculated thermodynamic parameters (Table 4) support the data and suggest a non-spontaneous sorption process which may require external energy input. This was supported by the positive $\Delta H°$ value which indicates an endothermic process though not at higher

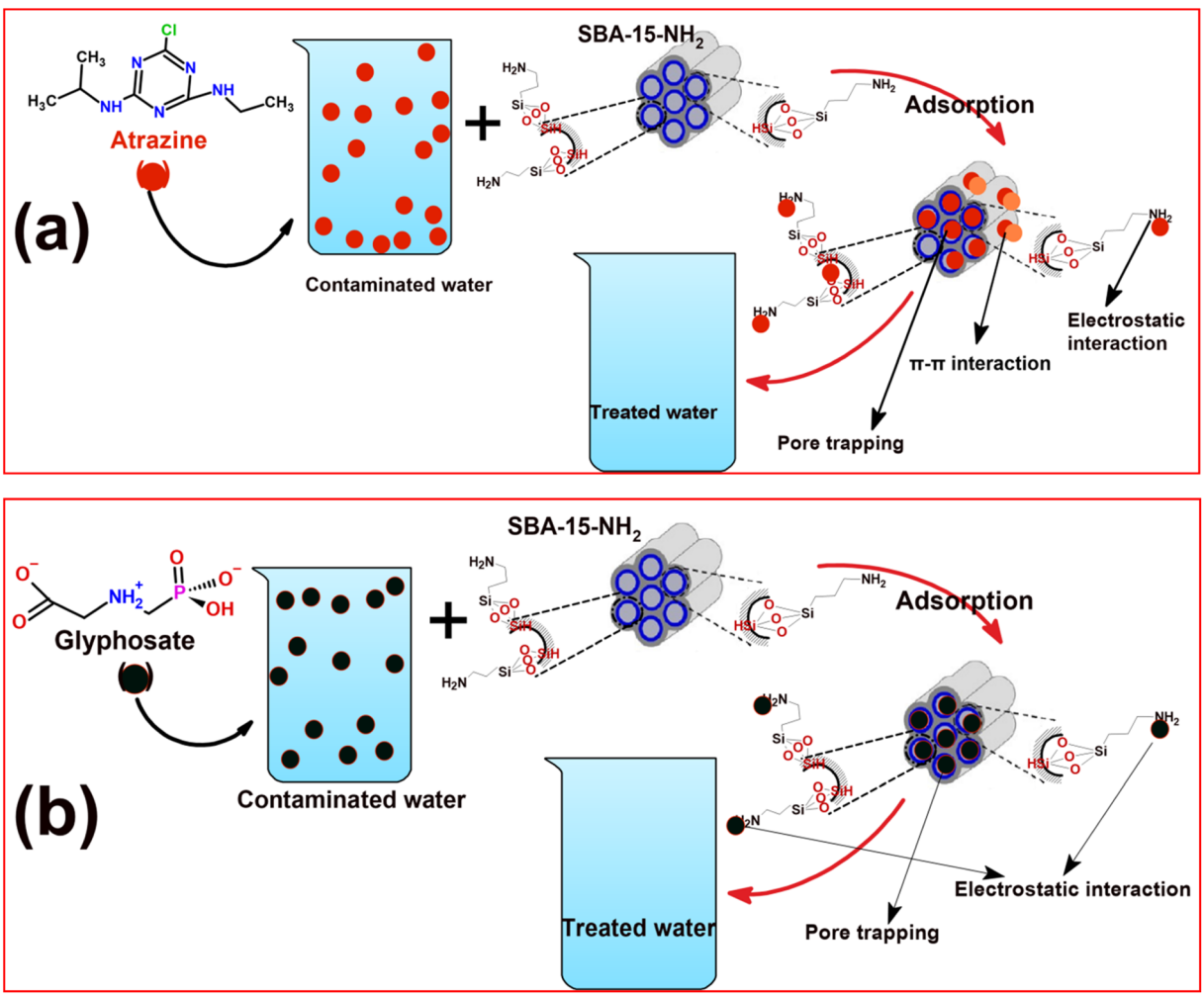

Fig. 5 Schematic of the adsorption process and the predicted contaminant uptake mechanism for (a) atrazine; (b) glyphosate.

Table 5 Comparison of adsorption capacities for atrazine and glyphosate

Adsorbent	Contaminant	Maximum q_e (μg g^{-1})	Reference
Cyclodextrin-modified polyacrylonitrile nanofiber	Atrazine	817	46
Co-pyrolyzed corn straw and sawdust biochar	Atrazine	37 200	47
Rice husk hydrochar	Atrazine	4060	48
Laser-induced graphitic material (LIG)	Atrazine	15 000	49
Heat treated kerolites	Atrazine	2291	50
Fullerenes	Atrazine	≈4100	51
ZIF-8 MOF	Atrazine	6780	40
Uio-67 MOF	Atrazine	10 960	40
Organo-beidellite	Atrazine	300	52
Magnetic multi-walled carbon nanotubes	Atrazine	40 160	53
MgO-modified leaf biochar	Atrazine	22 400	54
SBA-15-NH_2	Atrazine	145.13	This study
Fe_3O_4-coated trimethyl chitosan	Glyphosate	3040	55
Graphene–$MnFe_2O_4$	Glyphosate	6780	56
Kaolinite	Glyphosate	≈7900	57
Kaolinite–Humic acid composite	Glyphosate	≈8300	57
SBA-15-NH_2	Glyphosate	8756.5	This study
MWCNTS-MNPs	Glyphosate	21 170	58
Sep-CIPTES	Glyphosate	30 000	59
Calcined Ca–Al hydrotalcite	Glyphosate	41 000	60
CNT-MNP complex	Glyphosate	43 660	61
Biochar-nano-zero-valent iron (BC-NZVI)	Glyphosate	≈50 000	62
Cellulose activated carbon	Glyphosate	61 400	63
PGOSBA	Glyphosate	67 940	64
RGO/Fe_3O_4	Glyphosate	70 080	65

sorption temperature as observed in Fig. 4b. The positive entropy change (ΔS°) value indicated increased randomness in the adsorbent–solution interface and an increased degree of freedom of atrazine in solution as temperature increased.

The reusability study of SBA-15-NH_2 for atrazine adsorption was investigated over several adsorption–desorption cycles by employing used SBA-15-NH_2 which was washed with pure acetonitrile and the result is presented in Fig. 4c. The adsorbent exhibited sustained adsorption efficiencies for atrazine which was ≥82% even after 3 cycles. The second and third reuse cycles expressed 88.2 and 82.5% efficiencies, respectively, and this result indicates that the SBA-15-NH_2 is chemically stable over three cycles and reusable with slight losses (≈6%) on each run. Schematics of the adsorption processes and the predicted contaminant uptake mechanism for atrazine and glyphosate are presented in Fig. 5. The SBA-15-NH_2 adsorption capacities for atrazine and glyphosate were compared with those of some other adsorbents reported in the literature as presented in Table 5. Comparatively, the adsorbent exhibited far higher adsorption performance for glyphosate (≈60 fold) than atrazine, and the adsorption performance, especially for glyphosate, was better than several others.

Conclusion

Amine-functionalized Santa Barbara Amorphous-15 silica (SBA-15-NH_2) was synthesized and employed for the adsorption of atrazine and glyphosate. The SBA-15-NH_2 remained mesoporous post-functionalization but the aminopropyl silane moiety blocked some of the pores reducing the surface area, pore volume, and size by ≈2.8, 2.3, and 23 folds as well as lowering the stability by ≈10% when compared to the SBA-15. The distinctive SBA-15 hydroxyls broad band disappeared post-functionalization marking the point of the aminopropyl silane moiety attachment. However, a stronger amide-I peak appeared.

Compared to the SBA-15-NH_2, pristine SBA-15 had no significant adsorption for both atrazine and glyphosate. The pesticides adsorption rates were high with over 85% of potential adsorption having occurred within the initial 180 min. The equilibria for atrazine and glyphosate adsorption were 60 and 360 min, respectively, and the rate data fit the FPSO and PSO models, accordingly. These indicate a complex adsorption process and one mainly controlled by electrostatic interaction, respectively. The complex process comprises electrostatic interaction, trapping of atrazine within mesopores, and multilayer adsorption of atrazine on surface adsorbed atrazine.

Atrazine adsorption was higher at lower solution pH with reduced adsorption as pH value was raised; a trend which supports the hypothesis of the involvement of electrostatic attraction in the atrazine sequestration process. Atrazine adsorption was partly concentration-dependent, and there was enhanced adsorption as temperature increased from 22 to 42 °C, but further increase in temperature resulted in lower adsorption compared to that recorded at 22 °C. The experimental data fitted the Langmuir adsorption isotherm model better than the Freundlich model.

The SBA-15-NH_2 adsorption capacity for atrazine and glyphosate was better than several adsorbents reported in literature, the adsorbent is reusable, and exhibited sustained efficiencies for atrazine which was ≥82% even after 3-cycles, an indication of chemical stability and reusability.

Author contributions

P. N. Diagboya: conceptualization, formal analysis, funding acquisition, investigation, methodology, project administration, resources, supervision, validation, writing – original draft, review & editing; J. Junck: formal analysis, methodology, resources, writing – review & editing; S. O. Akpotu: conceptualization, methodology, project administration, writing – review & editing; R.-A. Düring: formal analysis, funding acquisition, investigation, methodology, project administration, resources, supervision, validation, writing – review & editing. All authors have approved and contributed to the final manuscript.

Conflicts of interest

The authors declare that this study was funded by the Alexander von Humboldt (AvH) Foundation (Germany). The authors declare no competing interest.

Acknowledgements

We acknowledge the support of Alexander von Humboldt (AvH) Foundation (Germany) for granting PN Diagboya the Georg Förster Research grant for experienced researcher. We acknowledge the technical support of BJ Heyde (Justus Liebig University).

References

1 A. Gogoi, P. Mazumder, V. K. Tyagi, G. G. Tushara Chaminda, A. K. An and M. Kumar, Occurrence and fate of emerging contaminants in water environment: a review, *Groundw. Sustain. Dev.*, 2018, **6**, 169–180.

2 A. Maddalon, V. Galbiati, C. Colosio, S. Mandić-Rajčević and E. Corsini, Glyphosate-based herbicides: evidence of immune-endocrine alteration, *Toxicology*, 2021, **459**, 152851.

3 O. M. Strilbyska, S. A. Tsiumpala, I. I. Kozachyshyn, T. Strutynska, N. Burdyliuk, V. I. Lushchak and O. Lushchak, The effects of low-toxic herbicide Roundup and glyphosate on mitochondria, *EXCLI J.*, 2022, **21**, 183–196.

4 R. V. Xikhongelo, F. M. Mtunzi, P. N. Diagboya, B. I. Olu-Owolabi and R.-A. Düring, Polyamidoamine functionalized graphene oxide-SBA-15 mesoporous composite: adsorbent for aqueous arsenite, cadmium, ciprofloxacin, ivermectin and tetracycline, *Ind. Eng. Chem. Res.*, 2021, **60**, 3957–3968.

5 O. K. Borggaard and A. L. Gimsing, Fate of glyphosate in soil and the possibility of leaching to ground and surface waters: a review, *Pest Manage. Sci.*, 2008, **64**, 441–456.

6 L. A. Cragin, J. S. Kesner, A. M. Bachand, D. B. Barr, J. W. Meadows, E. F. Krieg and J. S. Reif, Menstrual cycle characteristics and reproductive hormone levels in women exposed to atrazine in drinking water, *Environ. Res.*, 2011, **111**, 1293–1301.

7 E. Tzanetou and H. Karasali, in *Pests, Weeds and Diseases in Agricultural Crop and Animal Husbandry Production*, ed. D. Kontogiannatos, A. Kourti and K. F. Mendes, IntechOpen, 2020, DOI: 10.5772/intechopen.93066.

8 W. A. Battaglin, M. T. Meyer, K. M. Kuivila and J. E. Dietze, Glyphosate and Its Degradation Product AMPA Occur Frequently and Widely in U.S. Soils, Surface Water, Groundwater, and Precipitation, *J. Am. Water Resour. Assoc.*, 2014, **50**, 275–290.

9 E. Okada, D. Pérez, E. De Gerónimo, V. Aparicio, H. Massone and J. L. Costa, Non-point source pollution of glyphosate and AMPA in a rural basin from the southeast Pampas, Argentina, *Environ. Sci. Pollut. Res.*, 2018, **25**, 15120–15132.

10 K. Guyton, D. Loomis, Y. Grosse, F. El Ghissassi, L. Benbrahim-Tallaa, N. Guha, C. Scoccianti, H. Mattock and K. Straif, International Agency for Research on Cancer Monograph Working Group ILF. Carcinogenicity of tetrachlorvinphos, parathion, malathion, diazinon, and glyphosate, *Lancet Oncol.*, 2015, **16**, 490–491.

11 M. J. Davoren and R. H. Schiestl, Glyphosate-based herbicides and cancer risk: a post-IARC decision review of potential mechanisms, policy and avenues of research, *Carcinogenesis*, 2018, **39**, 1207–1215.

12 A. Sophia and E. Lima, Removal of emerging contaminants from the environment by adsorption, *Ecotoxicol. Environ. Saf.*, 2018, **150**, 1–17.

13 P. N. Diagboya, B. I. Olu-Owolabi, F. M. Mtunzi and K. O. Adebowale, Clay-carbonaceous material composites: towards a new class of functional adsorbents for water treatment, *Surf. Interfaces*, 2020, **19**, 100506.

14 P. N. E. Diagboya and E. D. Dikio, Silica-based mesoporous materials; emerging designer adsorbents for aqueous pollutants removal and water treatment, *Microporous Mesoporous Mater.*, 2018, **266**, 252–267.

15 K. Dashtian, R. Zare-Dorabei, R. Jafarinia and M. Saghanejhad Tehrani, Application of central composite design for optimization of preconcentration and determination of La (III) ion in water samples using the SBA-15-HESI and SBA-15-HESI-Fe3O4-NPs sorbents, *J. Environ. Chem. Eng.*, 2017, **5**, 5233–5240.

16 S. Nazerdeylami and R. Zare-Dorabei, Simultaneous adsorption of Hg2+, Cd2+ and Cu2+ ions from aqueous solution with mesoporous silica/DZ and conditions optimise with experimental design: kinetic and isothermal studies, *Micro Nano Lett.*, 2019, **14**, 823–827.

17 P. N. Diagboya, F. M. Mtunzi, R.-A. Düring and B. I. Olu-Owolabi, Empirical assessment and reusability of an eco-friendly amine-functionalized SBA-15 adsorbent for aqueous ivermectin, *Ind. Eng. Chem. Res.*, 2021, **60**, 2365–2373.

18 P. N. Diagboya, B. I. Olu-Owolabi and K. O. Adebowale, Microscale scavenging of pentachlorophenol in water using amine and tripolyphosphate-grafted SBA-15 silica: batch and modeling studies, *J. Environ. Manage.*, 2014, **146**, 42–49.

19 T. X. Bui, S. Y. Kang, S. H. Lee and H. Choi, Organically functionalized mesoporous SBA-15 as sorbents for removal of selected pharmaceuticals from water, *J. Hazard. Mater.*, 2011, **193**, 156–163.

20 A. G. N. Wamba, G. P. Kofa, S. N. Koungou, P. S. Thue, E. C. Lima, G. S. dos Reis and J. G. Kayem, Grafting of Amine functional group on silicate based material as adsorbent for water purification: a short review, *J. Environ. Chem. Eng.*, 2018, **6**, 3192–3203.

21 L. Rivoira, M. Appendini, S. Fiorilli, B. Onida, M. Del Bubba and M. C. Bruzzoniti, Functionalized iron oxide/SBA-15 sorbent: investigation of adsorption performance towards glyphosate herbicide, *Environ. Sci. Pollut. Res.*, 2016, **23**, 21682–21691.

22 A. N. Ebelegi, N. Ayawei, D. Wankasi, E. D. Dikio, P. N. Diagboya and F. M. Mtunzi, Covalently bonded polyamidoamine functionalized silica used as a Pb(II) scavenger from aqueous solution, *J. Environ. Chem. Eng.*, 2019, **7**, 103214.

23 R. Rosal, M. S. Gonzalo, A. Rodríguez, J. A. Perdigón-Melón and E. García-Calvo, Catalytic ozonation of atrazine and linuron on MnOx/Al2O3 and MnOx/SBA-15 in a fixed bed reactor, *Chem. Eng. J.*, 2010, **165**, 806–812.

24 C. V. Waiman, M. J. Avena, M. Garrido, B. Fernández Band and G. P. Zanini, A simple and rapid spectrophotometric method to quantify the herbicide glyphosate in aqueous media. Application to adsorption isotherms on soils and goethite, *Geoderma*, 2012, **170**, 154–158.

25 P. R. Sera, P. N. Diagboya, S. O. Akpotu, F. M. Mtunzi and T. B. Chokwe, Potential of valourized Moringa oleifera seed waste modified with activated carbon for toxic metals decontamination in conventional water treatment, *Bioresour. Technol. Rep.*, 2022, **16**, 100881.

26 I. Langmuir, The constitution and fundamental properties of solids and liquids, *J. Am. Chem. Soc.*, 1916, **38**, 2221–2295.

27 H. M. F. Freundlich, Über die adsorption in lösungen, *Z. fur Phys. Chem.*, 1906, **57**(57), 385–470.

28 P. S. Ghosal and A. K. Gupta, Determination of thermodynamic parameters from Langmuir isotherm constant-revisited, *J. Mol. Liq.*, 2017, **225**, 137–146.

29 E. C. Lima, A. Hosseini-Bandegharaei, J. C. Moreno-Piraján and I. Anastopoulos, A critical review of the estimation of the thermodynamic parameters on adsorption equilibria. Wrong use of equilibrium constant in the Van't Hoof equation for calculation of thermodynamic parameters of adsorption, *J. Mol. Liq.*, 2019, **273**, 425–434.

30 S. O. Akpotu, I. A. Lawal, B. Moodley and A. E. Ofomaja, Covalently linked graphene oxide/reduced graphene oxide-methoxylether polyethylene glycol functionalised silica for scavenging of estrogen: adsorption performance and mechanism, *Chemosphere*, 2020, **246**, 125729.

31 Q. Tao, Z. Xu, J. Wang, F. Liu, H. Wan and S. Zheng, Adsorption of humic acid to aminopropyl functionalized SBA-15, *Microporous Mesoporous Mater.*, 2010, **131**, 177–185.

32 M. Haerifar and S. Azizian, Fractal-like kinetics for adsorption on heterogeneous solid surfaces, *J. Phys. Chem.*, 2014, **118**, 1129–1134.

33 S. O. Akpotu, P. N. Diagboya, I. A. Lawal, S. O. Sanni, A. Pholosi, F. M. Mtunzi and A. E. Ofomaja, Designer composite of montmorillonite-reduced graphene oxide-PEG polymer for water treatment: enrofloxacin sequestration and cost analysis, *Chem. Eng. J.*, 2023, **453**, 139771.

34 I. Lupul, J. Yperman, R. Carleer and G. Gryglewicz, Adsorption of atrazine on hemp stem-based activated carbons with different surface chemistry, *Adsorption*, 2015, **21**, 489–498.

35 L. Yue, C. Ge, D. Feng, H. Yu, H. Deng and B. Fu, Adsorption–desorption behavior of atrazine on agricultural soils in China, *J. Environ. Sci.*, 2017, **57**, 180–189.

36 B. Prado, C. Duwig, C. Hidalgo, K. Müller, L. Mora, E. Raymundo and J. D. Etchevers, Transport, sorption and degradation of atrazine in two clay soils from Mexico: Andosol and Vertisol, *Geoderma*, 2014, **232–234**, 628–639.

37 P. N. Diagboya, B. I. Olu-Owolabi and K. O. Adebowale, Distribution and interactions of pentachlorophenol in soils: the roles of soil iron oxides and organic matter, *J. Contam. Hydrol.*, 2016, **191**, 99–106.

38 I. D. Kovaios, C. A. Paraskeva, P. G. Koutsoukos and A. C. Payatakes, Adsorption of atrazine on soils: model study, *J. Colloid Interface Sci.*, 2006, **299**, 88–94.

39 G. Abate and J. C. Masini, Adsorption of Atrazine, Hydroxyatrazine, Deethylatrazine, and Deisopropylatrazine onto Fe(III) Polyhydroxy Cations Intercalated Vermiculite and Montmorillonite, *J. Agric. Food Chem.*, 2005, **53**, 1612–1619.

40 I. Akpinar and A. O. Yazaydin, Adsorption of Atrazine from Water in Metal–Organic Framework Materials, *J. Chem. Eng. Data*, 2018, **63**, 2368–2375.

41 P. N. Diagboya, F. N. Mtunzi, K. O. Adebowale and B. I. Olu-Owolabi, Assessment of the effects of soil organic matter and iron oxides on the individual sorption of two polycyclic aromatic hydrocarbons, *Environ. Earth Sci.*, 2021, **80**, 227.

42 B. I. Olu-Owolabi, P. N. Diagboya, F. M. Mtunzi, K. O. Adebowale and R.-A. Düring, Empirical aspects of an emerging agricultural pesticide contaminant retention on two sub-Saharan soils, *Gondwana Res.*, 2022, **105**, 311–319.

43 F. N. Mtunzi, P. N. Diagboya, R.-A. During and B. I. Olu-Owolabi, Mesoporous SBA-15 Functionalized with G-5 Polyamidoamine: A Sustainable Adsorbent for Effective Sequestration of an Emerging Aqueous Contaminant, *ACS Appl. Nano Mater.*, 2021, **4**, 3052–3061.

44 B. I. Olu-Owolabi, P. N. Diagboya, F. M. Mtunzi and R.-A. Düring, Utilizing eco-friendly kaolinite-biochar composite adsorbent for removal of ivermectin in aqueous media, *J. Environ. Manage.*, 2021, **279**, 111619.

45 W. J. Weber Jr., P. M. McGinley and L. E. Katz, A distributed reactivity model for sorption by soils and sediments. 1. Conceptual basis and equilibrium assessments, *Environ. Sci. Technol.*, 1992, **26**, 1955–1962.

46 M. B. Chabalala, M. Z. Al-Abri, B. B. Mamba and E. N. Nxumalo, Mechanistic aspects for the enhanced adsorption of bromophenol blue and atrazine over cyclodextrin modified polyacrylonitrile nanofiber membranes, *Chem. Eng. Res. Des.*, 2021, **169**, 19–32.

47 Y. Gao, Z. Jiang, J. Li, W. Xie, Q. Jiang, M. Bi and Y. Zhang, A comparison of the characteristics and atrazine adsorption capacity of co-pyrolysed and mixed biochars generated

from corn straw and sawdust, *Environ. Res.*, 2019, **172**, 561–568.
48 K. A. Phan, D. Phihusut and N. Tuntiwiwattanapun, Preparation of rice husk hydrochar as an atrazine adsorbent: optimization, characterization, and adsorption mechanisms, *J. Environ. Chem. Eng.*, 2022, **10**, 107575.
49 M. Bayati, M. Numaan, A. Kadhem, Z. Salahshoor, S. Qasim, H. Deng, J. Lin, Z. Yan, C.-H. Lin and M. Fidalgo de Cortalezzi, Adsorption of atrazine by laser induced graphitic material: an efficient, scalable and green alternative for pollution abatement, *J. Environ. Chem. Eng.*, 2020, **8**, 104407.
50 E. González-Pradas, x Socı, M. as-Viciana, M. Saifi, M. D. Ureña-Amate, F. Flores-Céspedes, M. Fernández-Pérez and M. Villafranca-Sánchez, Adsorption of atrazine from aqueous solution on heat treated kerolites, *Chemosphere*, 2003, **51**, 85–93.
51 K. Gai, B. Shi, X. Yan and D. Wang, Effect of Dispersion on Adsorption of Atrazine by Aqueous Suspensions of Fullerenes, *Environ. Sci. Technol.*, 2011, **45**, 5959–5965.
52 E. Grundgeiger, Y. H. Lim, R. L. Frost, G. A. Ayoko and Y. Xi, Application of organo-beidellites for the adsorption of atrazine, *Appl. Clay Sci.*, 2015, **105–106**, 252–258.
53 W.-W. Tang, G.-M. Zeng, J.-L. Gong, Y. Liu, X.-Y. Wang, Y.-Y. Liu, Z.-F. Liu, L. Chen, X.-R. Zhang and D.-Z. Tu, Simultaneous adsorption of atrazine and Cu (II) from wastewater by magnetic multi-walled carbon nanotube, *Chem. Eng. J.*, 2012, **211–212**, 470–478.
54 Y. Cao, S. Jiang, Y. Zhang, J. Xu, L. Qiu and L. Wang, Investigation into adsorption characteristics and mechanism of atrazine on nano-MgO modified fallen leaf biochar, *J. Environ. Chem. Eng.*, 2021, **9**, 105727.
55 S. F. Soares, C. O. Amorim, J. S. Amaral, T. Trindade and A. L. Daniel-da-Silva, On the efficient removal, regeneration and reuse of quaternary chitosan magnetite nanosorbents for glyphosate herbicide in water, *J. Environ. Chem. Eng.*, 2021, **9**, 105189.
56 P. Marin, R. Bergamasco, A. N. Módenes, P. R. Paraiso and S. Hamoudi, Synthesis and characterization of graphene oxide functionalized with MnFe2O4 and supported on activated carbon for glyphosate adsorption in fixed bed column, *Process Saf. Environ. Prot.*, 2019, **123**, 59–71.
57 F. Guo, M. Zhou, J. Xu, J. B. Fein, Q. Yu, Y. Wang, Q. Huang and X. Rong, Glyphosate adsorption onto kaolinite and kaolinite-humic acid composites: experimental and molecular dynamics studies, *Chemosphere*, 2021, **263**, 127979.
58 J. C. Diel, D. S. P. Franco, A. V. Igansi, T. R. S. Cadaval, H. A. Pereira, I. D. S. Nunes, C. W. Basso, M. D. C. M. Alves, J. Morais, D. Pinto and G. L. Dotto, Green synthesis of carbon nanotubes impregnated with metallic nanoparticles: characterization and application in glyphosate adsorption, *Chemosphere*, 2021, **283**, 131193.
59 H. B. Junior, E. da Silva, M. Saltarelli, D. Crispim, E. J. Nassar, R. Trujillano, V. Rives, M. A. Vicente, A. Gil, S. A. Korili, E. H. de Faria and K. J. Ciuffi, Inorganic–organic hybrids based on sepiolite as efficient adsorbents of caffeine and glyphosate pollutants, *Appl. Surf. Sci.*, 2020, **1**, 100025.
60 G. Peng, B. Tang and X. Zhou, Effect of Preparation Methods on the Adsorption of Glyphosate by Calcined Ca–Al Hydrotalcite, *ACS Omega*, 2021, **6**, 15742–15749.
61 J. C. Diel, D. S. P. Franco, I. D. S. Nunes, H. A. Pereira, K. S. Moreira, T. A. de L. Burgo, E. L. Foletto and G. L. Dotto, Carbon nanotubes impregnated with metallic nanoparticles and their application as an adsorbent for the glyphosate removal in an aqueous matrix, *J. Environ. Chem. Eng.*, 2021, **9**, 105178.
62 X. Jiang, Z. Ouyang, Z. Zhang, C. Yang, X. Li, Z. Dang and P. Wu, Mechanism of glyphosate removal by biochar supported nano-zero-valent iron in aqueous solutions, *Colloids Surf., A*, 2018, **547**, 64–72.
63 Q. Chen, J. Zheng, Q. Yang, Z. Dang and L. Zhang, Insights into the Glyphosate Adsorption Behavior and Mechanism by a MnFe2O4@Cellulose-Activated Carbon Magnetic Hybrid, *ACS Appl. Mater. Interfaces*, 2019, **11**, 15478–15488.
64 P. N. Diagboya, B. J. Heyde and R.-A. Düring, Efficient decontamination of aqueous glyphosate using Santa Barbara Amorphous-15 (SBA-15) and graphene oxide-SBA-15 poly-amidoamine functionalized composites, *Chem. Eng. J.*, 2023, 143263, DOI: **10.1016/j.cej.2023.143263**.
65 Y. Li, C. Zhao, Y. Wen, Y. Wang and Y. Yang, Adsorption performance and mechanism of magnetic reduced graphene oxide in glyphosate contaminated water, *Environ. Sci. Pollut. Res.*, 2018, **25**, 21036–21048.